Study of the Effect of the Floating Die Compaction on Mechanical Properties of Titanium Foams

Sergio Sauceda [1],*[iD]**, Sheila Lascano** [1][iD]**, Luis Béjar** [2]**, Guilherme O. Neves** [3][iD]**,
Ernesto Chicardi** [4][iD]**, Christopher Salvo** [5][iD] **and Claudio Aguilar** [6],*[iD]

[1] Departamento de Ingeniería Mecánica, Universidad Técnica Federico Santa María,
   Avenida Vicuña Mackenna 3939, Santiago 8940572, Chile; sheila.lascano@usm.cl
[2] Facultad de Ingeniería Mecánica, Universidad Michoacana de San Nicolás de Hidalgo, Ciudad Universitaria,
   Morelia 58000, Mexico; luis.bejar@umich.mx
[3] Laboratório de Materiais, Universidade Federal de Santa Catarina, Campus Trindade, Florianopolis,
   SC 88040-900, Brazil; guilherme.o.neves@labmat.ufsc.br
[4] Departamento de Ingeniería y Ciencia de los Materiales y del Transporte, Escuela Politécnica Superior,
   Calle Virgen de África 7, 41011 Sevilla, Spain; echicardi@us.es
[5] Departamento de Ingeniería Mecánica, Facultad de Ingeniería, Universidad del Bío-Bío, Avda. Collao 1202,
   Casilla 5-C, Concepción 4081112, Chile; csalvo@ubiobio.cl
[6] Departamento de Ingeniería Metalúrgica y de Materiales, Universidad Técnica Federico Santa María,
   Avenida España 1680, Valparaíso 2390123, Chile
*   Correspondence: sergio.sauceda@usm.cl (S.S.); claudio.aguilar@usm.cl (C.A.)

Abstract: Titanium (Ti) and its alloys are used for biomedical applications because of their high resistance to corrosion, good strength-to-weight ratio, and high fatigue resistance. However, a problem that compromises the performance of the material is the mismatch between Young's modulus of Ti and the bone, which brings about stress shielding. One strategy that has been investigated to reduce this difference is the manufacture of Ti-based foams, using powder metallurgy (PM) methods, such as the space-holder technique. However, in the uniaxial compaction, both non-uniform density distribution and mechanical properties remain because of the compaction method. This work studies the influence of compaction by adopting a floating-action die related to a single-action die (SAD), on the density of green and sintered Ti foams with porosities around 50 vol.% characterized by optical microscopy, ultrasound analysis, compression tests, and microhardness. The compaction process employing a floating-action die generates Ti foams with a higher density up to 10% with more control of the spacer particle added compared to the single-action die. Furthermore, compaction method has no relevant effect on microhardness and Young's modulus, which allows getting better consolidated samples with elastic modules similar to those of human bone.

Keywords: biomaterial; compaction; floating die; powder metallurgy; foam

1. Introduction

Titanium (Ti) is one of the metallic elements with the greatest development in recent decades because of its favorable strength-to-weight ratio, low thermal expansion coefficient, and good corrosion resistance [1]. For these aspects, titanium and its alloys have been used in the automotive, aerospace, marine, biomedical implant industries, among others [2,3].

Concerning to biomaterials, Ti and its alloys are one of the most suitable materials for their excellent behavior in the human body, derived from their outstanding balance between mechanical properties and biocompatibility [4]. Thus, commercially pure titanium (cp-Ti or titanium grade IV) is the usual biomaterial employed to fabricate dental implants for clinical use, to solve dental problems,

like periodontal diseases, trauma, genetic dental anomalies, and dentin dysplasia with the hereditary origin [5,6]. The Ti6Al4V alloy (also called titanium grade V) is used as a biomaterial for orthopedics implants [7,8] because of its superior mechanical strength and lower Young´s modulus in comparison with cp-Ti.

However, despite their widespread use as a biomaterial for bone replacement implants, both materials, i.e., cp-Ti grade IV and Ti6Al4V grade V, exhibit some handicaps, such as inadequate fatigue strength, a higher stiffness compared to human bone tissues, and excessive micromovements in the implant-bone tissue interface for the bioinert nature of Ti [9,10], that make around 10% of bone implants fail during the first 5 years post-implantation [11,12]. In addition, the toxicity of both Al and V in the Ti6Al4V can cause biological issues, such as deficient bone mineralization, fertility decrease, fetotoxicity, and teratogenicity, among other important health complications [13–16].

Thus, one of the most relevant handicaps of those traditional metallic biomaterials for bone implants is based on the stiffness mismatch between the bone tissues (Young's modulus, E, around 1 GPa and 20–25 GPa for trabecular and bone tissue [16]) and the implant of Ti and Ti6Al4V materials (100–110 GPa). This imbalance in mechanical loads influences bone remodeling and increases bone formation in the heaviest zones and decreases it in areas with no gravitation. The areas with fewer stimuli present lower bone density, which favors premature fractures and the loosening of the implants [17–19].

A potential solution to mitigate the stress-shielding effect phenomenon is the manufacture of functional materials with a controlled porosity designed to reduce Young's modulus of the materials, such as metal foams, addressed by the scientific community [20,21]. From the implant point of view, the metallic foams have high-energy absorption capacity because they can allow higher deformation before reaching their yield strength, increasing the area under the stress-strain curve [22], in the same way that a structure with open pores provides channels for bone ingrowth and neovascularization, which promotes the osseointegration process [23,24].

There are different ways to obtain Ti foams [21], such as grow of pressurized gas bubbles [25], additive manufacturing [26], and replication [27], among the alternatives [28]. However, the space-holder technique is one of the powder metallurgy (PM) methods, which is extensively used for their simplicity generate porous structures needed for metallic foams [29], permitting to control the size and distribution of the pores [30]. In this method, the metallic powders are mixed with a spacer particle that is compacted in an uniaxial way, and the space-holder particles are eliminated by dissolution or thermal treatment [31]. The space-holder must be selected based on the following criteria: (i) size and shape, (ii) cost, (iii) Ti reactivity with it, and (iv) easy process ability, among alternatives [32,33]. Afterward, the porous green compacts are sintered, generating the coalescence of the powder particles [34].

However, uniaxial compaction made with a single-action die (SAD) requires a higher amount of energy to improve the foam matrix densification [35]. A feasible solution to address this issue is the search for better densification of the metallic structure to generate a specimen with greater mechanical strength and a controlled porosity.

There are different methods to generate metallic foams with improved apparent density distribution on the compact, such as cold compaction with double-effect machines, hot-pressing [32], or spark plasma sintering [36]. However, these techniques involve very high costs and specialized infrastructure compared to the conventional PM process.

For cylindrical compaction die with removable upper and lower punches, there are two different compaction methods, uniaxial and biaxial. In the uniaxial method, the die is kept stationary, and it applies a force to a punch, thus consolidating the material in a green compact [37]. However, this method promotes a non-homogeneous distribution of the compaction pressure in the green specimen. In addition, friction with the walls of the matrix generates a density profile in the sample [38–40]. For the biaxial method, there are two options: (i) the double-effect compaction and (ii) using a floating die (FD). In the double-effect compaction, a stationary die is applied, and the compaction forces are

applied by an upper punch and a lower punch. The disadvantage of this method is that a double-acting press is required, which has a very high cost and is not common in research laboratories. In FD compaction, a device is used which adapts to a single-acting press, without the need to replace existing machinery. In the compaction with a floating die (FD), the pressure employed to the upper punch is distributed to both punches, the lower and the upper, generating a biaxial effect similar to that of a double-effect, thus bringing about a more homogeneous density profile.

Some authors studied the effect of a floating die (FD) in bulk samples produced by the PM route [41–44]. The densification profile behavior with FD in commercial aluminum solids was investigated by H. Homayoun et al. [35], comparing them with single-action die (SAD) compacted samples. S. T. Hong et al. [45] investigated the stress profiles of a floating die (FD) during the compaction of both commercially Pure titanium (cp-Ti) and Fe powders showing that the FD simulates compaction die with double effect. B. A. Behrens [46] showed that more homogeneous density profiles are achieved in cylindrical samples manufactured from TiAl6V4 powders with FDs. However, it is still necessary to study the bringing about of the density profile on the porosity and mechanical properties in metallic foams.

In this sense, different models are applied to predict Young's modulus in Ti foams and alloys, considering the density, porosity, and experimental constants [47]. Almost all analytical models are based on some ideal microstructures of the pores that give rise to being able to calculate properties from geometric analysis. One of the most utilized is the proposed by Gibson and Ashby [48] with the equation (1) shown in Table 1, where E_s and ρ_s are Young's modulus and the theoretical density of titanium, E and ρ are the values of the metal foam, and C and n are constant between 0.2 to 1.6 for C and 1.4 to 4.8 for n in metal foams [31]. This model makes a correlation between the pores, treating them as defined polyhedrons. With the relative density of the material, these polyhedrons behave with empty faces for interconnected pore foams as in this study. According to the type of pore, other criteria are applied.

Table 1. Young's modulus prediction models.

Model	Equation	Constants Used	References
$\frac{E}{E_s} = C\left(\frac{\rho}{\rho_s}\right)^n$	(1)	C = 1, n = 2.96	[48,49]
$\frac{E}{E_s} = e^{-bP}$	(2)	B = 3.5	[50,51]
$\frac{E}{E_s} = 1 - e^{-r(1-P)}$	(3)	r = 0.5	[52]
$\frac{E}{E_s} = \left(1 - UP^{\frac{2}{3}}\right)^s$	(4)	U = 1.3; s = 1.2	[47,53]

Another model is proposed by Knudsen (1959) and Spriggs (1961) [50,51,54]; see Equation (2). In this model, porosity (P) of foam is related in an exponential function, and b is a constant between 1 and 9. This model is composed of a systematic arrangement of spheres of equal size intercepting each other to simulate junction necks, is based on the theory of grain structure, and is used with moderate levels of porosity.

Rice (1976) [52] suggested another model based on generalize of the Knudsen and Spriggs equation; see Equation (3). In contrast to the previous model where there are spheres of the same size which, as the porosity increases, agglomerate more of these equal spheres leaving a greater quantity of solid between pores, this model uses a variable spherical pore radius, in a way that, by increasing the size of each pore, the total porosity increases, and, therefore, the pore distance is reduced, thus reducing the matrix area and increasing the pore area. Another model is introduced by Boccaccini et al. (1993) [53], creating their model of Equation (4). This spheroidal pore model defined, with this, the effective Young's modulus can be correlated as a function of the volume fraction of closed porosity, the shape of the pores (axial ratio of the spheroidal pores), and their orientation.

In addition, hardness depends on the density and porosity of metal foams [55,56]. The densification of samples obtained by PM techniques is influenced by the bonding between the powder particles and

the less microporosity generated. Reported measurements of microhardness show values between 3.1 GPa and 3.8 GPa for commercial Ti6Al4V obtained by casting and wrought [57] and 5.3–7.355 GPa for Ti6Al2Co foams obtained by space-holder technique and other PM processes [56,58].

In this work, the effect of biaxial flotation die compaction on the density and Young's modulus of titanium foams manufactured using the space-holder technique was studied. For this purpose, it was necessary to design and manufacture a floating die (FD) with a biaxial effect that can be adapted to any universal testing machine or compaction press. The effect of FD compaction on the porosity, densification, and mechanical properties of pure titanium foams is studied and compared with that produced by a single-action die (SAD).

2. Materials and Methods

2.1. Floating Die (FD) Design and Manufacturing

A device was designed and manufactured to adapt the Zwick/Roell Z030 universal machine (Zwick/Roell GmbH & Co. KG, Ulm, Germany) to operate with a floating die (FD), as shown in Figure 1. This device comprises an upper punch, a static lower punch, a die supported on a platform, and two springs (damping system). In this study, cylindrical specimens of 8 mm in diameter and up to 20 mm in height were obtained.
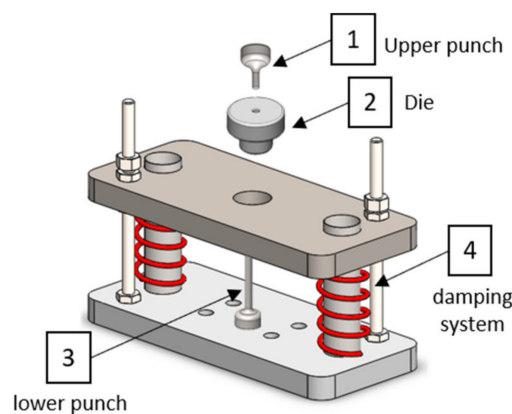
Figure 1. Designed device for floating die (FD) process.

The design of the structure that supports the die consists of two plates of AISI 1045 steel, 25.4 mm of thickness. The lower one was assembled to the universal machine and held in place by four M8 hexagon screws. The compaction die was in the upper plate. Two cylindrical bars of AISI 1020, 25.4 mm in diameter, were placed as guides for the metal springs of 28.6 mm in diameter, 24-mm thick wire, and 100-m length. These bars were lubricated to allow the sliding of the upper plate. Two M10 screws were added to adjust the level and height of the upper plate due to the nuts to position the plate, according to American Society for Testing and Materials ASTM E2014–17.

2.2. Synthesis of Ti Foams

The experiments were carried out employing cp-Ti grade IV powders (99.5% pure, -350 mesh), supplied by NOAH Technologies Co. (San Antonio, TX, USA). Mechanical milling was carried out for 2 h in a RETSCH®PM 400 planetary mill using YSZ (Yttria-Stabilized Zirconia) milling media. This step was implemented to increase the compressibility of powders without effect in its structure [59,60].

Then, the milled powders were weighed and mixed in a RETSCH®MM400 (Retsch GmbH, Hann, Germany) mixer mill for 30 min at 30 Hz with ammonium carbonate (NH_4HCO_3) particles, distributed by Winkler Ltda. (Winkler Ltda., Santiago, Chile), to generate porous structures with porosities around 0%, 30%, 40%, and 50 vol.% and pore sizes between 100 μm and 500 μm of diameter.

To obtain the samples' weight (Table 2), Equations (5) and (6) were used, where the % vol. of NH_4HCO_3 added is taken as a reference to calculate the mass of Ti powder and spacer particles:

$$m_{Ti} = 0.9 \cdot \rho_{Ti} \cdot \left(1 - \frac{\% \text{ spacer particle added}}{100}\right) \cdot V, \tag{5}$$

$$m_{NH_4HCO_3} =]\rho_{NH_4HCO_3} \cdot \left(\frac{\% \text{ spacer particle added}}{100}\right) \cdot V, \tag{6}$$

where m_{Ti} and $m_{NH_4HCO_3}$ are the calculated mass values for Titanium and Ammonium Carbonate; ρ_{Ti} and $\rho_{NH_4HCO_3}$ represent the density of Ti and ammonium carbonate with values of 4.51 and 1.5 g·cm^{-3}. It is considered that the conventional PM technique does not achieve total densification, so the experimental factor of 0.9 is added. Finally, V represents the volume of cylindrical samples of 8 mm in diameter and 10 mm in height were obtained. Subsequently, the blends were compacted and sintered as shown in Figure 2.

Table 2. Mass of powders used for different porosities of the Ti foams (SA: Simple-action and FA: Floating-action dies).

Spacer Particle Added (vol.%)	Weight of Ti Powder (g)	Weight of NH₄HCO₃ Powder (g)
0% SA 0% FA	1.632	0.0
30% SA 30% FA	1.143	0.181
40% SA 40% FA	0.979	0.241
50% SA 50% FA	0.816	0.302
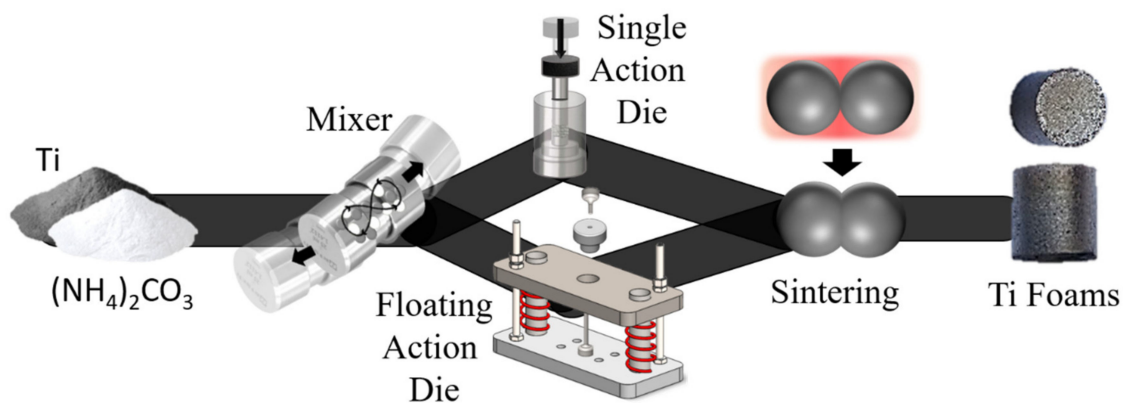
Figure 2. Scheme of the metal foam manufacturing process using the space-holder technique and the flotation compaction device. Note that the single-action die (SAD) device was also applied in a parallel route to compare and evaluate the flotation compaction device result.

Two compaction methods were applied to compare its effect on the densification, porosity, and mechanical response (Young's modulus, compressive yield strength, and microhardness): (i) the uniaxial compaction with a single die Figure 3a and (ii) the biaxial compaction with the FD (Figure 3b). In both cases, the lower punch remains stationary, but in the case of the FD, the friction between the die walls and the powder causes the die to descend and moves to the lower punch. Both dies and their respective punches were fabricated of steel T1 tool speed W18Cr4V. Zinc stearate powder was used as a solid lubricant on the walls of the die and punches. For powder compaction (Ti and space-holder particles),

the configuration shown in Figure 3 was placed in a ZwickRoell Z030 (Zwick/Roell GmbH & Co. KG , Ulm, Germany) universal machine, and a compaction pressure of 550 MPa was applied during a dwell time of 1 min. After compaction, the green compacts were subjected to a two-stage heat treatment in a Nabertherm P330 horizontal tube ceramic furnace (Nabertherm GmbH, Lilienthal, Germany) using a flow of pure argon of 1.25 L·min^{-1} as the inert atmosphere. They were first heated-up up to 180 °C for 3 h to remove the space-holder from the green samples, and then the temperature was raised to the sintering temperature of 1250 °C for 3 h. The heating ramp of 5 °C·min^{-1} was applied between each stage.
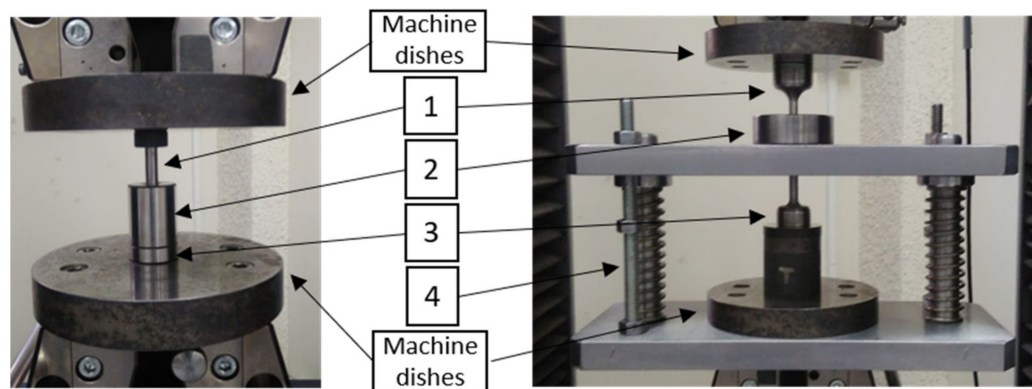
Figure 3. Compaction devices used: (**a**) Single-action die; (**b**) floating-action die. (1) upper punch; (2) die; (3) lower punch; (4) damping system.

2.3. Microstructural and Mechanical Characterization

For the measurement of density and porosity, the Archimedes method was carried out with immersion in distilled water following ASTM B962–17, where the apparent density and total porosity of the sample were estimated. Three samples for each percentage spacer particle added were obtained, and both compaction method. For each sample, measures were repeated three times to estimate the mean value of the density, and statistical analysis was performed by t-student test. The interconnected porosity was calculated from the density measurements, according to the ASTM C373 standard.

For the metallographic study, the samples were prepared using a sequence of cutting, resin mounting, grinding, and polishing, corresponding the ASTM E2014-17. Optical microscopy (OM) was carried out to observe the porosity distribution with a Leica DM500 microscope (Leica Microsystems, Mannheim, Germany). A collage with 15 images taken at 50× per piece was made to obtain a complete top view of the transversal section of the porous specimens, assembled by using Adobe Illustrator CS6 software version 21.0.0 (Adobe Systems Incorporated, San Jose, CA, United States). The densification obtained by both compaction methods was studied.

As a result, using the densities and porosities obtained from the Archimedes test, Young's modulus was estimated based on different models: Gibson and Ashby [48], Knudsen and Spriggs [50,51,54], Rice [52], and Boccaccini et al. (1993) [53]. For the Gibson and Ashby model were used the constants C = 1 and n = 2.96 proposed by Mansourighasri et al. [49]; for titanium foams made by the space-holder technique; and for Knudsen and Spriggs' model was employed the constant b = 3.5 for cold-compressed and sintered foams [51].

Furthermore, uniaxial compression tests were carried out, in cylindrical specimens with a radius height/diameter of 0.8, according to the ASTM E9-89a standard. The tests were carried out with a compression speed of 0.005 m/m-min with a preload of 10 N and one sample for each percentage of porosity for each compaction method. Compliance in the load elements, such as supports and cell load, was considered. The analyses were executed randomly to eliminate errors induced by variables [61], such as size of the sample, location of the sensor, torsional compliance, or stiffness of the test machine [62–65]. Dynamic Young's modulus was estimated by using the ultrasound technique

using a 20 MHz frequency with a WaveSurfer Digital Storage 432 oscilloscope from the company Teledyne LeCroy™ and a 3.175 mm transducer.

Finally, microhardness testing was carried out on the titanium matrix to evaluate the influence of porous structure on the micromechanical properties of samples [55,56], by using microhardness tester ZHVμ distributed by ZwickRoell GmbH & Co.KG (Ulm, Germany). The distance between the indentation measurements points and the closest pore was twice that of the size of the indentation. Thirty measures per sample were used to calculate the mean value of the hardness on the sample, with a load of 0.2 HV in the titanium matrix. Statistical analysis was performed to verify the normality in the distribution of the raw data by applying a Shapiro–Wilk test for the 30 measures per sample. Then, a t-student test was applied for the microhardness measurements with a normal distribution, to analyze if significant differences were found between the compared compaction methods. For non-normal data, a Mann–Whitney U test was performed for the scattered data.

3. Results and Discussions

The results of Archimedes´ method for the green compacts and the sintered samples are presented in Figure 4a,b. The effect of the content of spacer particles added and the two compaction methods used on the densities is analyzed. In Figure 4a, it is noted that the green compact density decreases with the increase in the spacer added (0, 30, 40, or 50 vol.% of NH_4HCO_3). In addition, it is noticeable that when using the floating-action die, a rise of 3% on average in the density is observed, which causes an increase by up to 11% of the density in the sintered titanium foams.
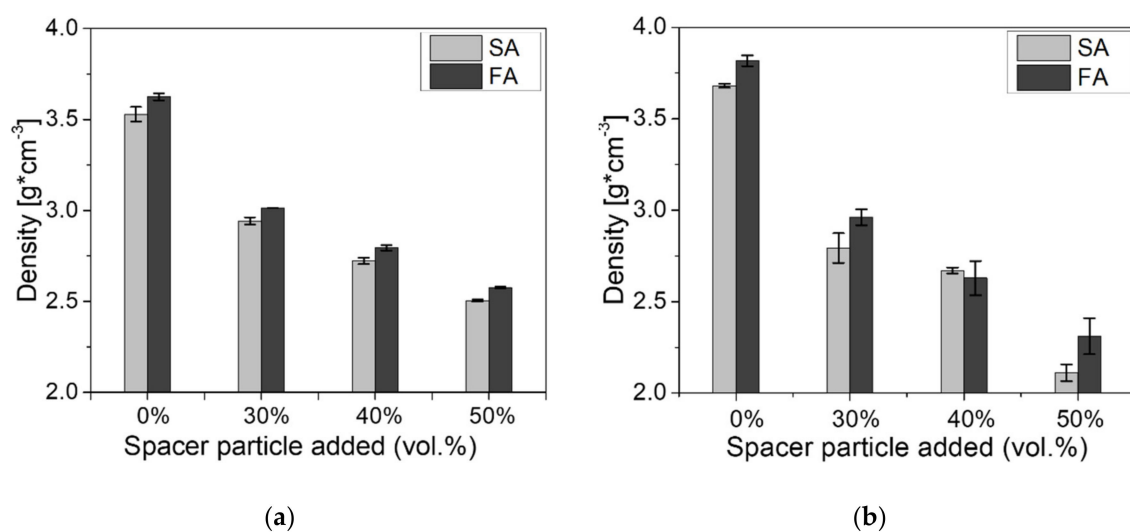

(a)   (b)

Figure 4. Density of titanium foams obtained: (**a**) Green samples; (**b**) sintered samples.

The statistical results of the comparison of the density produced by each compaction method before and after sintering are shown in Table 3. As it is observed, for the green samples, the variation in density between both compaction methods is statistically significant ($P_{value} < 0.05$), being higher in the foams with floating action. It is the result of the movement of die resulting from friction between the walls of the die and the powder particles which causes a relative displacement between the die and lower punch, distributing the total load between the upper and lower punch. It is observed that this difference remains significant even after sintering, except for the cases with 40 vol.% of NH_4HCO_3, with $P_{value} > 0.05$, where the density is the same in both methods due to a higher standard deviation in the density measurements for the samples with a floating matrix (Table 3). This is due to the fact of lower densification of green samples compacted via simple action die promotes a high contraction during the sintering process. The foams compressed with a floating action matrix present a tendency to maintain a higher density.

Table 3. Comparison of means between densities according to the compaction methods, SA: Simple-action and FA: Floating-action dies.

Spacer Particle Added (vol.%)	Cases	Green Density (g·cm^{-3})	P$_{value}$ ($\alpha = 0.05$)	Sintered density (g·cm^{-3})	P$_{value}$ ($\alpha = 0.05$)
0% SA	3	3.53	0.0035	3.68	0.0005
0% FA	3	3.62		3.82	
30% SA	3	2.94	0.0005	2.79	0.0079
30% FA	3	3.01		2.96	
40% SA	3	2.72	0.0008	2.67	0.2635
40% FA	3	2.79		2.63	
50% SA	3	2.50	0.0000	2.11	0.0069
50% FA	3	2.58		2.31	

The percentage values of interconnected porosity for the sintered samples obtained as a function of the percentage of space-holder used is shown in Figure 5. For the samples compacted by FD, the interconnected porosity is closer to the spacer added, and density values are higher than those obtained for the samples compacted with the use of simple action die, so there is less microporosity. This effect is very positive for possible biomedical applications of Ti foams, since the greater the interconnected porosity, and the potential of cell growth within the implant (bone in-growth) [23].
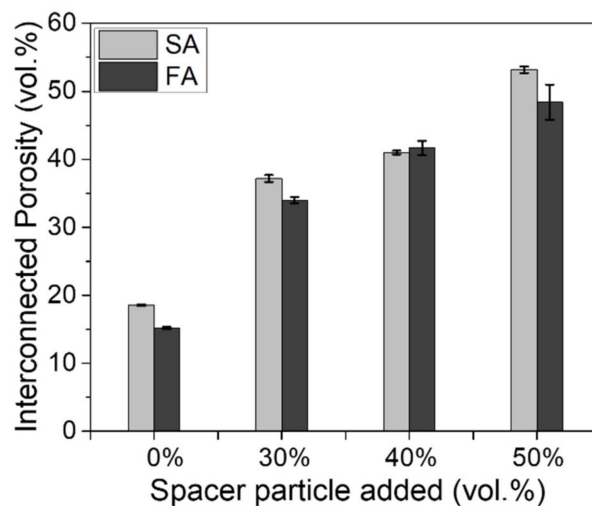
Figure 5. Interconnected porosity as a function of the vol.% of ammonium carbonate used as spacer particle.

OM micrographs of cp-Ti porous samples obtained by the space-holder technique and compacted by single-action (SA) and FA, are depicted in Figure 6. All the porous specimens produced with both compacting methods exhibited a non-uniform bimodal distribution of the macropores and micropores. Interconnected pores with significant size distributions are observed, which are associated with the wide size range of the space-holder particles applied (from 35 μm to 810 μm and irregular morphology). Larger pore size was obtained by comparing to the expected size, which may be related to the high hygroscopic behavior of the spacer used, allowing it to absorb humidity from the environment during the compaction process and producing agglomeration of the spacer particles before the sintering process, resulting in larger pores.

In addition, higher amount of microporosity (attributed to the PM method) is observed in the samples compacted by the single-action die (SAD) (Figure 6a) compared with those compacted with double effect die (Figure 6b). This effect is observed for both the 30 vol.%, and 40 vol.% of NH_4HCO_3 (Figure 6c–f). However, the high porosity of the samples with 50% of ammonium carbonate, does not allow us to appreciate this effect (Figure 6g,h). It is also noted that the pressed samples with FD have a

higher density at the edges, regardless of the spacer particle added, which gives better mechanical stability and handling in the green compacts (Figure 6h).
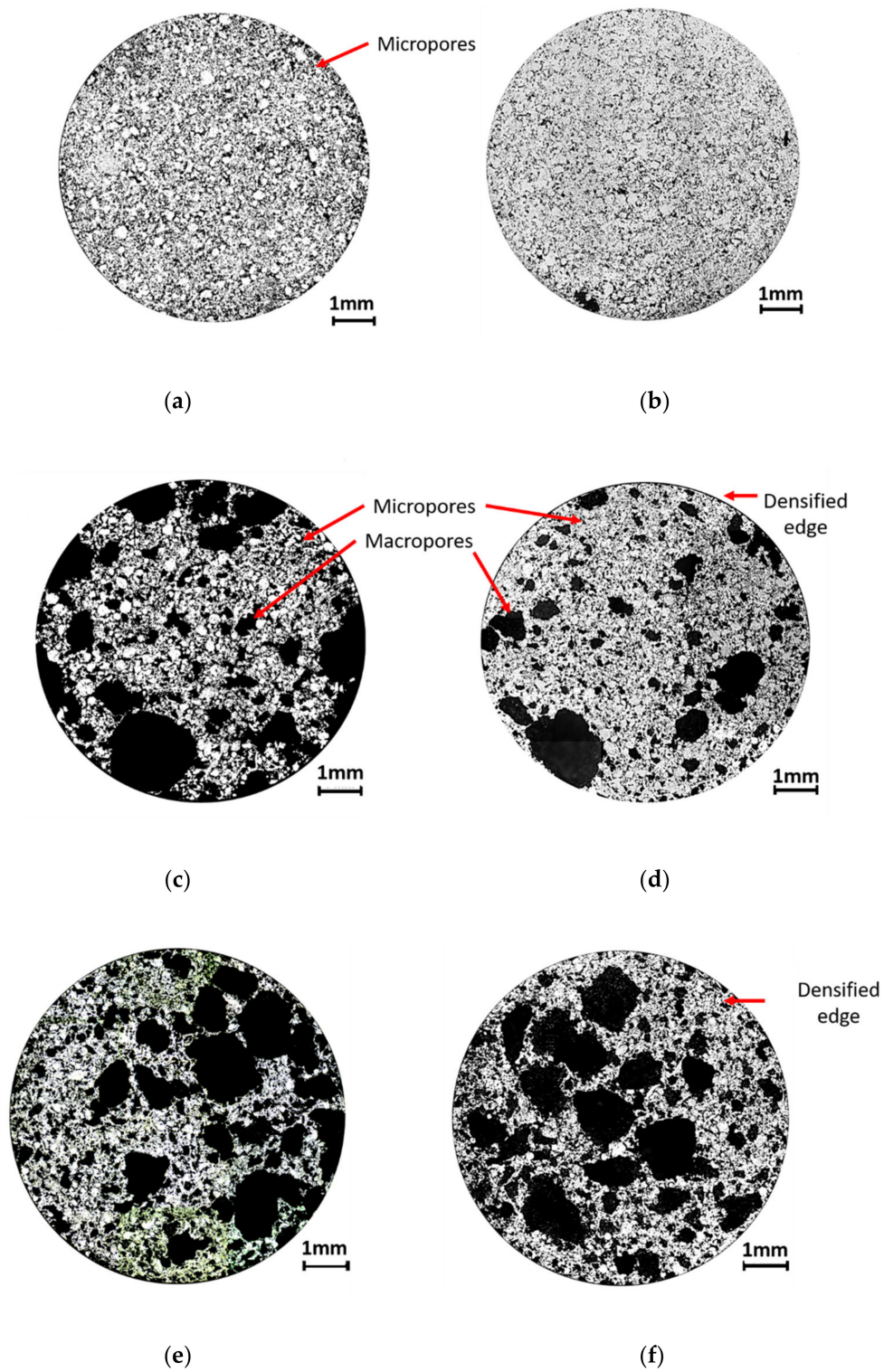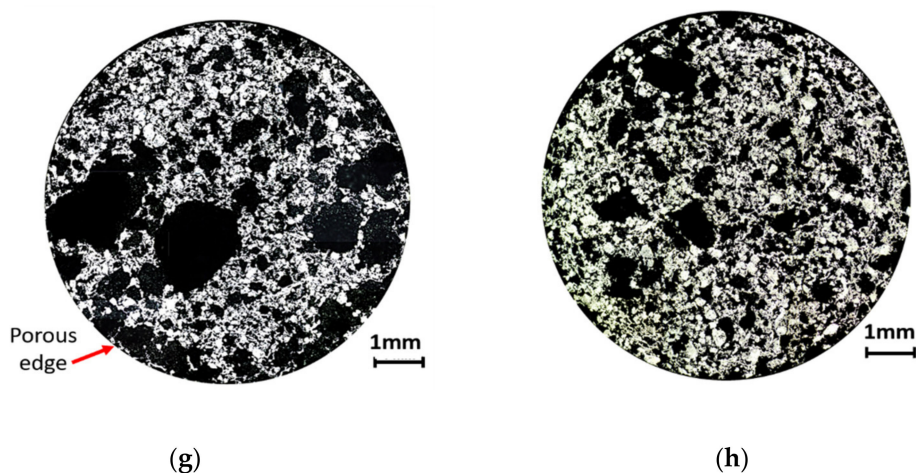

(**a**)　　　　　　　　　　　　　　　　　　　(**b**)

(**c**)　　　　　　　　　　　　　　　　　　　(**d**)

(**e**)　　　　　　　　　　　　　　　　　　　(**f**)

Figure 6. *Cont.*

(**g**)   (**h**)

Figure 6. Microstructure images at 50x of Ti porous samples compacted with single-action die (SAD) with porosity of (**a**) 0%, (**c**) 30%, (**e**) 40%, and (**g**) 50%; and compacted with a floating-action die with porosity of (**b**) 0%, (**d**) 30%, (**f**) 40%, and (**h**) 50%.

A prediction of Young's modulus was made using different models reported in the literature for porous structures: Gibson and Ashby [48], Knudsen and Spriggs [50,51], Rice [52], and Boccaccini et al. [53]. Figure 7 shows Young's modulus calculated utilizing the mentioned models. The results show that, Young's modulus increases for the compacted samples with floating-action die, except for those with 40 vol.% of NH_4HCO_3 because the density and porosity values used to calculate them do not present a difference between both methods (SA and FA). These results were compared with those obtained by using ultrasonic testing and the uniaxial compression test. For ultrasound measurements, it was not possible to determine Young's modulus for foams because the high porosity causes the sound wave, when entering a pore, to be damped by decreasing its amplitude and causing an unreliable reading. For samples with 0% of NH_4HCO_3, Young's modulus obtained by FD and simple effect die was 57 GPa and 47 GPa.
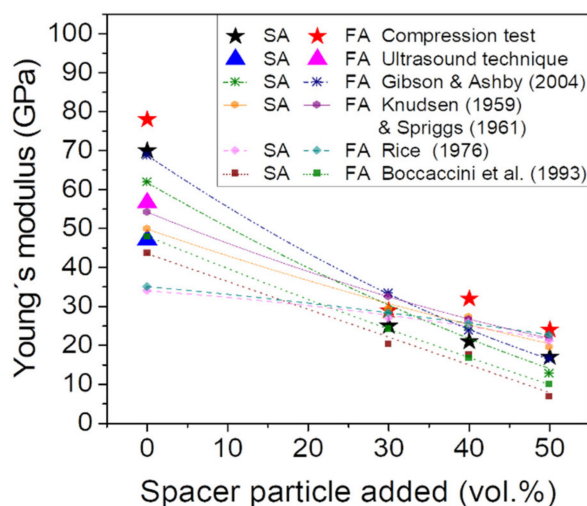
Figure 7. Young's modulus prediction with different models.

In general, the model with better predictions concerning Young's modulus achieved experimentally, was proposed by Gibson and Ashby, with an error percentage between 11% to 33%. It should be mentioned that Young's modulus predicted by Knudsen and Spriggs model is the closest to the dynamic Young's modulus obtained by ultrasound technique (US), with an error rate of 15%. For measures obtained experimentally, the error was between 3% to 55%. The Young's modulus estimated with

models are summarized in Table 4. Other authors performed finite element analysis (FEA) to predict and test the properties of Ti foams produced by using ammonium carbonate as space-holder particles. They suggested three different models to simulate the pores, which provides good results in the predictions; however, these present considerable overestimation on Ti foams with higher porosity, being necessary to use distinct models for each porosity ranges [66].

Table 4. Young's modulus predicted with different models.

| Method of Compaction	Spacer Particle Added (vol.%)	Compression Test (GPa)	Ultrasound Technique (GPa)	Gibson and Ashby (GPa)	Knudsen and Spriggs (GPa)	Rice (GPa)	Boccaccini et al. (GPa)
Simple action die	0%	70	56.6	62	50	34	44
	30%	25	-	28	29	27	20
	40%	21	-	25	27	26	17
	50%	17	-	13	19	21	6
Floating-action die	0%	78	47.1	69	54	35	48
	30%	29	-	33	32	28	24
	40%	32	-	24	27	25	17
	50%	24	-	16	22	23	10

The physical and mechanical properties obtained for the different porous sample configurations are summarized in Table 5. As expected, the lowest porosity and the highest Young's modulus were obtained for cp-Ti samples with 0 vol.% of NH_4HCO_3. In general, highest Young's modulus are obtained for specimens pressed by using a floating-action die, compared with those compacted by a single-action die (SAD). Despite achieving a reduction of approximately 30% in their mechanical properties with this technique for Ti in bulk (110 GPa), which can be caused by combining two effects: remaining porosity resulting from low compaction pressure and incomplete sintering, Young's modulus are closer to the values of human cortical bone (~30 GPa) [66].

**Table 5.** Summary of properties of titanium foams.

Method of Compaction	Spacer Particle Added (vol.%)	Interconnected Porosity Pint (%)	Total Porosity P (%)	Relative Density ($\rho_{apparent}/\rho_{Ti}$)	Yield Strength (MPa)	Young's Modulus (GPa)
Simple action die	0%	18.6 ± 0.1	26.4 ± 0.2	0.82	387	70
	30%	39.2 ± 0.6	44.1 ± 0.6	0.62	29	25
	40%	41.0 ± 0.3	46.6 ± 0.2	0.59	20	21
	50%	53.0 ± 0.6	57.8 ± 0.3	0.47	24	17
Floating-action die	0%	15.2 ± 0.2	23.7 ± 0.2	0.85	337	78
	30%	34.5 ± 0.6	40.8 ± 0.2	0.66	42	29
	40%	41.5 ± 1.1	47.4 ± 0.2	0.58	29	32
	50%	49.8 ± 2.7	53.8 ± 1.4	0.51	16	24

The mechanical response of cp-Ti porous samples was analyzed by uniaxial compression tests and the results of the compression stress vs strain curves are shown in Figure 8 shows. For the titanium foams, a reduction in Young's modulus is obtained until reaching a range between 15% and 23% for the die with single-action (Figure 8a) regarding Ti in bulk, and 22% to 29% for the floating-action die (Figure 8b).

The variation of Young's modulus and yield strength as a function of relative density is illustrated in Figure 9. An increase in the relative density for all the samples does not lead to an increase in Young's modulus analyzing all samples, as is observed in Figure 9a. In terms of Young's modulus, there is no significant difference between the results obtained by the two compaction methods with values between 21 and 32 GPa, close to cortical bone. In addition, by increasing the spacer particle added a greater interconnected porosity is achieved, but it does not weaken the titanium matrix. This can be explained because of the mechanical properties have been influenced by the higher densification of the samples obtained by the compaction process, generating a greater resistant area due to a better distribution of porosity. Regarding the yield strength, Figure 9b shows that, for FA die compacted samples, there is a constant rise with little variation as the densification increases for samples with spacer particle added, while SA die samples do not have a defined behavior.

(**a**)　　　　　　　　　　　　　　　　　　　　(**b**)
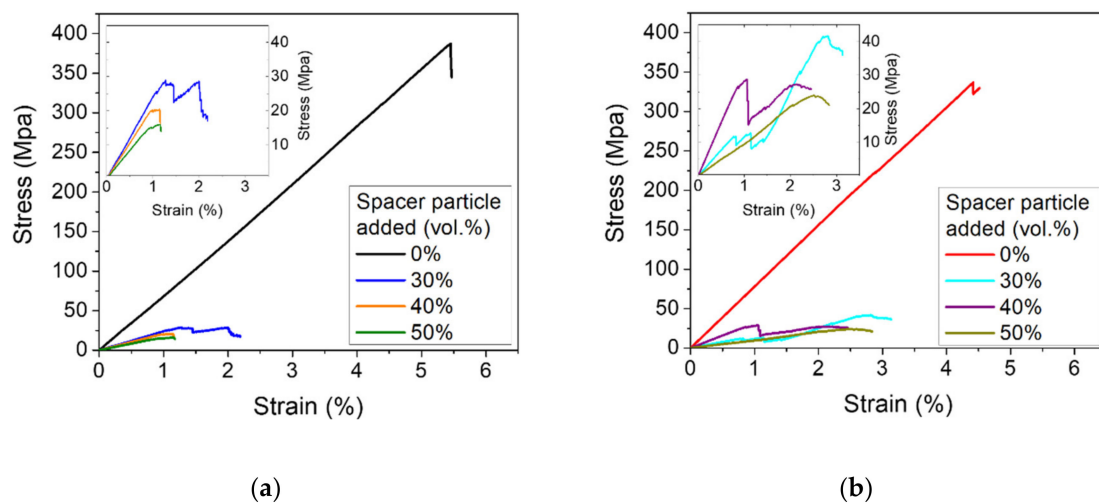
Figure 8. Stress-strain curves of compression test (**a**) simple-action die (SA) and (**b**) floating-action (FA) die.


(**a**)　　　　　　　　　　　　　　　　　　　　(**b**)
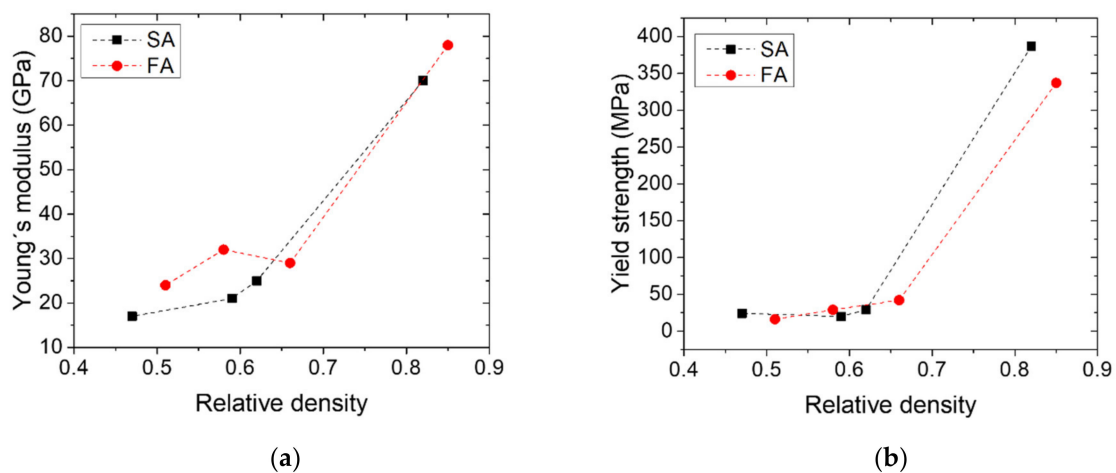
Figure 9. Variation of (**a**) Young's modulus and (**b**) yield strength, as a function of relative density.

These measures do not necessarily tend to increase when density rises; however, it is relevant that they remain in the same order of magnitude. Therefore, the floating-action die would comply with the manufacture of more consolidated parts without having a rise in Young's modulus of the titanium foams.

The results of the microindentation test are presented in Figure 10. The microhardness measurements are studied in function of the compaction method (SA and FA) and are represented in a box chart with the average values and the dispersion of these data (Figure 10a). It is seen that the area of the boxes for all the porosities falls in the same range of microhardness measures, which suggests that, although there is a numerical difference of the rates, it does not present a clear tendency of improvement in the microhardness by using a floating die (FD). Although Young's modulus of the samples is below those reported for Ti in bulk, there is no change in microhardness of tested specimens, which indicates a homogeneous sintering in all samples regardless of the compaction method. The indentations were placed in the matrix keeping in mind an appropriate distance between the pores, which acting as stress raisers (Figure 10b).

Finally, the statistical results for microhardness distribution are summarized in Table 6. In all cases, the distribution $p < 0.5$ value shows that the group of indentations made for the Ti-foams produced by compacting with FD does not present a statistical difference with those compacted with

simple-action die. However, the mean values are higher than reported for Ti6Al4V obtained by casting and wrought [57] and Ti alloys [58].

(**a**)　　　　　　　　　　　　　　　　　　　　　　　　(**b**)
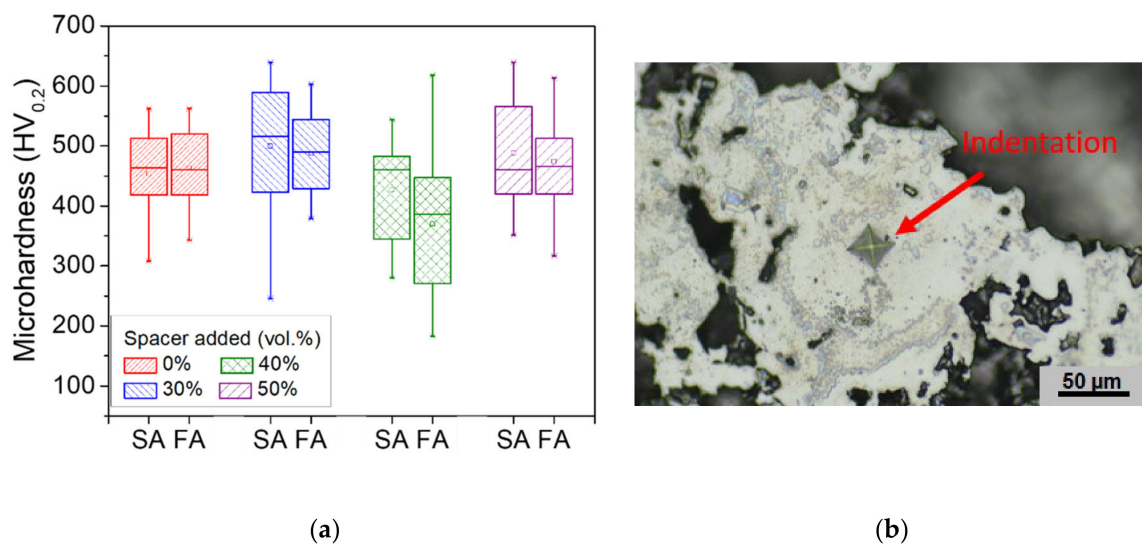
Figure 10. Microhardness measurement: (**a**) Distribution box plot, (**b**) indentation of microhardness measurement of 40% FA sample.

Table 6. Results of statistical analysis and mean value of microhardness according to the compaction method.

Sample	Significance of Normality	Type of Test	P_{value} ($\alpha = 0.05$)	Microhardness ($HV_{0.2}$)	Microhardness (GPa)
0% SA	0.107	T student	0.399	447	4.384
0% FA	0.544	Mann-Whitney		465	4.560
30% SA	0.039	Mann-Whitney	0.482	483	4.737
30% FA	0.421	Mann-Whitney		478	4.688
40% SA	0.008	Mann-Whitney	0.126	411	4.031
40% FA	0.334	Mann-Whitney		370	3.629
50% SA	0.214	T-student	0.408	477	4.678
50% FA	0.153	T-student		455	4.462

4. Conclusions

We compared compacted titanium foams with floating-action and simple action dies and studied the effect on the densification and how it affects the porosity, microhardness, yield strength, and Young's modulus, obtaining the following conclusions.

The compacting process assisted by a floating-action die generates parts with higher densification compared with the simple-action die because of the better distribution of the compression forces through the green specimen. In general, this increase in density prevails even after the sintering process, which allows generation of metal foams with greater stability.

The compaction process via floating-action die produces lower microporosity than those obtained by simple action compaction. Therefore, there is further control of the porosity by using space-holder technique with cold compaction.

There is no relevant effect of the compaction method on microhardness, yield strength, and Young's modulus, which allows obtaining better-consolidated samples without affecting their mechanical properties.

Author Contributions: All the authors have been contributed to obtain a high-quality research work. S.S.: investigation, validation, analysis of the results and writing original draft preparation, S.L.: writing- original draft, review and editing, L.B.: writing original draft preparation, funding acquisition, G.O.N.: investigation, validation, supervised fabrication processes and writing original draft, E.C.: review and editing, discussion of the

Conflicts of Interest: The authors declare no conflict of interest.

References

1. Zhou, L.; Yuan, T.; Tang, J.; He, J.; Li, R. Mechanical and corrosion behavior of titanium alloys additively manufactured by selective laser melting—A comparison between nearly β titanium, α titanium and α + β titanium. *Opt. Laser Technol.* **2019**, *119*, 105625. [CrossRef]

2. Yue, X.-Z.; Fukazawa, H.; Kitazono, K. Strain rate sensitivity of open-cell titanium foam at elevated temperature. *Mater. Sci. Eng. A* **2016**, *673*, 83–89. [CrossRef]

3. Kulshreshtha, A.; Dhakad, S. *Preparation of Metal Foam by Different Methods: A Review*; Elsevier: Amsterdam, The Netherlands, 2020; Volume 26, pp. 1784–1790.

4. Kaur, M.; Singh, K. Review on titanium and titanium based alloys as biomaterials for orthopaedic applications. *Mater. Sci. Eng. C* **2019**, *102*, 844–862. [CrossRef]

5. Tallarico, M.; Cervino, G.; Scrascia, R.; Uccioli, U.; Vaira, L.A.; Meloni, S.M. Minimally Invasive Treatment of Edentulous Maxillae with Overdenture Fully Supported by a Cad/Cam Titanium Bar with a Low-Profile Attachment Screwed on Four or Six Implants: A Case Series. *Prosthesis* **2020**, *2*, 6. [CrossRef]

6. Martín-González, J.; Sánchez-Domínguez, B.; Tarilonte-Delgado, M.; Castellanos-Cosano, L.; Llamas-Carreras, J.; López-Frías, F.; Segura-Egea, J.J. Anomalías y displasias dentarias de origen genético-hereditario. *Av. Odontoestomatol.* **2012**, *28*, 287–301. [CrossRef]

7. Niinomi, M. Mechanical biocompatibilities of titanium alloys for biomedical applications. *J. Mech. Behav. Biomed. Mater.* **2008**, *1*, 30–42. [CrossRef]

8. Elias, C.N.; Fernandes, D.J.; De Souza, F.M.; Monteiro, E.D.S.; De Biasi, R.S. Mechanical and clinical properties of titanium and titanium-based alloys (Ti G2, Ti G4 cold worked nanostructured and Ti G5) for biomedical applications. *J. Mater. Res. Technol.* **2019**, *8*, 1060–1069. [CrossRef]

9. Tschernitschek, H.; Borchers, L.; Geurtsen, W. Nonalloyed titanium as a bioinert metal—A review. *J. Prosthet. Dent.* **2006**, *96*, 12. [CrossRef]

10. Nicholson, J.W. Titanium Alloys for Dental Implants: A Review. *Prosthesis* **2020**, *2*, 11. [CrossRef]

11. Schwarz, M.S. Mechanical complications of dental implants. *Clin. Oral Implant. Res.* **2000**, *11*, 156–158. [CrossRef]

12. Hernandez-Rodriguez, M.; Contreras-Hernandez, G.; Juarez-Hernandez, A.; Beltran-Ramirez, B.; Garcia-Sanchez, E. Failure analysis in a dental implant. *Eng. Fail. Anal.* **2015**, *57*, 236–242. [CrossRef]

13. Klein, G. Aluminum toxicity to bone: A multisystem effect? *Osteoporos. Sarcopenia* **2019**, *5*, 2–5. [CrossRef]

14. Wilk, A.; Szypulska-Koziarska, D.; Wiszniewska, B. The toxicity of vanadium on gastrointestinal, urinary and reproductive system, and its influence on fertility and fetuses malformations. *Postępy Higieny i Medycyny Doświadczalnej* **2017**, *71*, 850–859. [CrossRef] [PubMed]

15. Ghosh, S.K.; Saha, R.; Saha, B.B. Toxicity of inorganic vanadium compounds. *Res. Chem. Intermed.* **2015**, *41*, 4873–4897. [CrossRef]

16. Zhang, L.-C.; Chen, L.-Y. A Review on Biomedical Titanium Alloys: Recent Progress and Prospect. *Adv. Eng. Mater.* **2019**, *21*. [CrossRef]

17. Shirazi, H.A.; Ayatollahi, M.R.; Asnafi, A. To reduce the maximum stress and the stress shielding effect around a dental implant–bone interface using radial functionally graded biomaterials. *Comput. Methods Biomech. Biomed. Eng.* **2017**, *20*, 750–759. [CrossRef]

18. Wang, P.; Todai, M.; Nakano, T. Beta titanium single crystal with bone-like elastic modulus and large crystallographic elastic anisotropy. *J. Alloy. Compd.* **2019**, *782*, 667–671. [CrossRef]

19. Kourtis, S.; Damanaki, M.; Kaitatzidou, S.; Kaitatzidou, A.; Roussou, V. Loosening of the fixing screw in single implant crowns: Predisposing factors, prevention and treatment options. *J. Esthet. Restor. Dent.* **2017**, *29*, 233–246. [CrossRef]

20. Lascano, S.; Arévalo, C.; Montealegre-Melendez, I.; Muñoz, S.; Rodriguez-Ortiz, J.A.; Trueba, P.; Torres, Y. Porous Titanium for Biomedical Applications: Evaluation of the Conventional Powder Metallurgy Frontier and Space-Holder Technique. *Appl. Sci.* **2019**, *9*, 982. [CrossRef]

21. Trueba, P.; Chicardi, E.; Rodriguez-Ortiz, J.A.; Torres, Y. Development and implementation of a sequential compaction device to obtain radial graded porosity cylinders. *J. Manuf. Process.* **2020**, *50*, 142–153. [CrossRef]

22. Xiao, L.; Song, W.; Wang, C.; Liu, H.; Tang, H.; Wang, J. Mechanical behavior of open-cell rhombic dodecahedron Ti–6Al–4V lattice structure. *Mater. Sci. Eng. A* **2015**, *640*, 375–384. [CrossRef]

23. Hong, J.-Y.; Ko, S.-Y.; Lee, W.; Chang, Y.-Y.; Kim, S.-H.; Yun, J.-H. Enhancement of Bone Ingrowth into a Porous Titanium Structure to Improve Osseointegration of Dental Implants: A Pilot Study in the Canine Model. *Materials* **2020**, *13*, 3061. [CrossRef]

24. Pałka, K.; Pokrowiecki, R. Porous Titanium Implants: A Review. *Adv. Eng. Mater.* **2018**, *20*, 1700648. [CrossRef]

25. Murray, N.; Dunand, D.C. Effect of thermal history on the superplastic expansion of argon-filled pores in titanium: Part I kinetics and microstructure. *Acta Mater.* **2004**, *52*, 2269–2278. [CrossRef]

26. Yuan, L.; Ding, S.; Wen, C. Additive manufacturing technology for porous metal implant applications and triple minimal surface structures: A review. *Bioact. Mater.* **2019**, *4*, 56–70. [CrossRef] [PubMed]

27. Ryan, G.; Pandit, A.; Apatsidis, D.P. Fabrication methods of porous metals for use in orthopaedic applications. *Biomaterials* **2006**, *27*, 2651–2670. [CrossRef]

28. Singh, R.; Lee, P.D.; Dashwood, R.J.; Lindley, T.C. Titanium foams for biomedical applications: A review. *Mater. Technol.* **2010**, *25*, 127–136. [CrossRef]

29. Arifvianto, B.; Zhou, J. Fabrication of Metallic Biomedical Scaffolds with the Space Holder Method: A Review. *Materials* **2014**, *7*, 3588–3622. [CrossRef]

30. Zheng, J.-P.; Chen, L.-J.; Chen, D.-Y.; Shao, C.-S.; Yi, M.-F.; Zhang, B. Effects of pore size and porosity of surface-modified porous titanium implants on bone tissue ingrowth. *Trans. Nonferrous Met. Soc. China* **2019**, *29*, 2534–2545. [CrossRef]

31. Jha, N.; Mondal, D.; Majumdar, J.D.; Badkul, A.; Jha, A.K.; Khare, A. Highly porous open cell Ti-foam using NaCl as temporary space holder through powder metallurgy route. *Mater. Des.* **2013**, *47*, 810–819. [CrossRef]

32. Salvo, C.; Aguilar, C.; Guzman, D.; Alfonso, I.; Mangalaraja, R. Mechanically enhanced novel Ti-based alloy foams obtained by hot pressing. *Mater. Sci. Eng. A* **2019**, *759*, 112–123. [CrossRef]

33. Khodaei, M.; Meratian, M.; Savabi, O. Effect of spacer type and cold compaction pressure on structural and mechanical properties of porous titanium scaffold. *Powder Met.* **2015**, *58*, 152–160. [CrossRef]

34. Sharma, M.; Gupta, G.K.; Dasgupta, R.; Kumar, M.; Kumar, P. Titanium Foams Processed Through Powder Metallurgy Route Using Lubricant Acrawax as Space Holder Material. *Trans. Indian Inst. Met.* **2018**, *71*, 1933–1940. [CrossRef]

35. Homayoun, H.; Shahbaz, M.; Ebrahimi, R. Investigation of Floating and Single-Action Dies in Producing Dense Compacts with High Aspect Ratio. *Iran. J. Sci. Technol. Trans. Mech. Eng.* **2019**, *44*, 1005–1011. [CrossRef]

36. Wang, Z.; Sun, H.; Du, Y.; Yuan, J. Effects of Powder Preparation and Sintering Temperature on Properties of Spark Plasma Sintered Ti-48Al-2Cr-8Nb Alloy. *Metals* **2019**, *9*, 861. [CrossRef]

37. Cristofolini, I.; Pederzini, G.; Rambelli, A.; Molinari, A. Densification and deformation during uniaxial cold compaction of stainless steel powder with different particle size. *Powder Met.* **2016**, *59*, 73–84. [CrossRef]

38. Molinari, A.; Cristofolini, I.; Pederzini, G.; Rambelli, A. A densification equation derived from the stress-deformation analysis of uniaxial cold compaction of metal powder mixes. *Powder Met.* **2018**, *61*, 210–218. [CrossRef]

39. Kadiri, M.; Michrafy, A.; Dodds, J. Pharmaceutical powders compaction: Experimental and numerical analysis of the density distribution. *Powder Technol.* **2005**, *157*, 176–182. [CrossRef]

40. Lee, S.; Kim, K. Densification behavior of aluminum alloy powder under cold compaction. *Int. J. Mech. Sci.* **2002**, *44*, 1295–1308. [CrossRef]

41. De Medeiros, J.P.; Hammes, G.; Neves, G.O.; Martinelli, A.E.; Klein, A.N.; Binder, C. Effect of Liquid Phase–Assisted Sintering on the Microstructure, Mechanical Properties, and Tribological Behavior of Self-Lubricating Ferrous Composites. *Adv. Eng. Mater.* **2020**, *22*. [CrossRef]

42. Mann, R.; Hexemer, R.; Donaldson, I.; Bishop, D. Hot deformation of an Al–Cu–Mg powder metallurgy alloy. *Mater. Sci. Eng. A* **2011**, *528*, 5476–5483. [CrossRef]

43. Neves, G.O.; Tirollo, H.G.; Probst, S.M.H.; Binder, C.; Klein, A.N. Application of computational thermodynamics to Fe/Ni, Fe-3%Si/Ni and 316L/Ni systems produced by powder metallurgy. *Powder Met.* **2017**, *60*, 301–308. [CrossRef]

44. Macaskill, I.A.; LaDepha, A.D.P.; Milligan, J.H.; Fulton, J.J.; Bishop, D. Effects of cold and hot densification on the mechanical properties of a 7XXX series powder metallurgy alloy. *Powder Met.* **2009**, *52*, 304–310. [CrossRef]

45. Hong, S.-T.; Hovanski, Y.; Lavender, C.A.; Weil, K.S. Investigation of Die Stress Profiles during Powder Compaction Using Instrumented Die. *J. Mater. Eng. Perform.* **2008**, *17*, 382–386. [CrossRef]

46. Behrens, B.-A.; Gastan, E.; Vahed, N. Application of tool vibration in die pressing of Ti-powder. *Prod. Eng.* **2010**, *4*, 545–551. [CrossRef]

47. Torres-Sanchez, C.; McLaughlin, J.; Bonallo, R. Effect of Pore Size, Morphology and Orientation on the Bulk Stiffness of a Porous Ti35Nb4Sn Alloy. *J. Mater. Eng. Perform.* **2018**, *27*, 2899–2909. [CrossRef]

48. Gibson, L.J.; Ashby, M.F. *Cellular Solids: Structure and Properties*, 2nd ed; Cambridge University Press: Cambridge, UK, 2014. [CrossRef]

49. Mansourighasri, A.; Muhamad, N.; Sulong, A.B. Processing titanium foams using tapioca starch as a space holder. *J. Mater. Process. Technol.* **2012**, *212*, 83–89. [CrossRef]

50. Knudsen, F.P. Dependence of Mechanical Strength of Brittle Polycrystalline Specimens on Porosity and Grain Size. *J. Am. Ceram. Soc.* **1959**, *42*, 376–387. [CrossRef]

51. Spriggs, R.M. Expression for Effect of Porosity on Elastic Modulus of Polycrystalline Refractory Materials, Particularly Aluminum Oxide. *J. Am. Ceram. Soc.* **1961**, *44*, 628–629. [CrossRef]

52. Rice, R.W. Extension of the Exponential Porosity Dependence of Strength and Elastic Moduli. *J. Am. Ceram. Soc.* **1976**, *59*, 536–537. [CrossRef]

53. Boccaccini, A.; Ondracek, G.; Mazilu, P.; Windelberg, D. On the Effective Young's Modulus of Elasticity for Porous Materials: Microstructure Modelling and Comparison between Calculated and Experimental Values. *J. Mech. Behav. Mater.* **1993**, *4*, 119–128. [CrossRef]

54. Torres, Y.; Lascano, S.; Bris, J.; Pavón, J.; Rodriguez, J.A. Development of porous titanium for biomedical applications: A comparison between loose sintering and space-holder techniques. *Mater. Sci. Eng. C* **2014**, *37*, 148–155. [CrossRef] [PubMed]

55. Murr, L.E.; Gaytan, S.M.; Medina, F.; Martinez, E.; Martinez, J.L.; Hernandez, D.H.; Machado, B.I.; Ramirez, D.A.; Wicker, R.B. Characterization of Ti-6Al-4V open cellular foams fabricated by additive manufacturing using electron beam melting. *Mater. Sci. Eng. A* **2010**, *527*, 1861–1868. [CrossRef]

56. Terrazas, C.A.; Murr, L.E.; Bermudez, D.; Arrieta, E.; Roberson, D.A.; Wicker, R.B. Microstructure and mechanical properties of Ti-6Al-4V-5% hydroxyapatite composite fabricated using electron beam powder bed fusion. *J. Mater. Sci. Technol.* **2019**, *35*, 309–321. [CrossRef]

57. Murr, L.E.; Quinones, S.; Gaytan, S.; Lopez, M.; Rodela, A.; Martinez, E.; Hernandez, D.; Medina, F.; Wicker, R. Microstructure and mechanical behavior of Ti–6Al–4V produced by rapid-layer manufacturing, for biomedical applications. *J. Mech. Behav. Biomed. Mater.* **2009**, *2*, 20–32. [CrossRef] [PubMed]

58. Abhash, A.; Singh, P.; Muchhala, D.; Kumar, R.; Gupta, G.K.; Mondal, D.P. Research into the change of macrostructure, microstructure and compressive deformation response of Ti6Al2Co foam with sintering temperatures and space holder contents. *Mater. Lett.* **2020**, *261*, 126997. [CrossRef]

59. Singh, P.; Abhash, A.; Yadav, B.N.; Shafeeq, M.; Singh, I.B.; Mondal, D.P. Effect of milling time on powder characteristics and mechanical performance of Ti4wt%Al alloy. *Powder Technol.* **2019**, *342*, 275–287. [CrossRef]

60. Restrepo, A.H.; Ríos, J.M.; Arango, F.; Correa, E.; Zuleta, A.A.; Valencia-Escobar, A.; Bolivar, F.J.; Castaño, J.G.; Echeverría, F.E. Characterization of titanium powders processed in n-hexane by high-energy ball milling. *Int. J. Adv. Manuf. Technol.* **2020**, *110*, 1681–1690. [CrossRef]

61. Montgomery, D.C. Design and Analysis of Experiments. *Technometrics* **2006**, *48*, 158. [CrossRef]

62. Gorham, D. An effect of specimen size in the high strain rate compression test. *Le J. Phys. IV* **1991**, *1*, C3-411–C3-418. [CrossRef]

63. Gedney, R. Measurement errors in mechanical testing. *Adv. Mater. Process.* **2007**, 301–325. [CrossRef]

64. Kalidindi, S.R.; Abusafieh, A.; El-Danaf, E. Accurate characterization of machine compliance for simple compression testing. *Exp. Mech.* **1997**, *37*, 210–215. [CrossRef]

65. Muñoz, S.; Castillo, S.; Torres, Y. Different models for simulation of mechanical behaviour of porous materials. *J. Mech. Behav. Biomed. Mater.* **2018**, *80*, 88–96. [CrossRef] [PubMed]

66. Cetinel, O.; Esen, Z.; Yildirim, B. Fabrication, Morphology Analysis, and Mechanical Properties of Ti Foams Manufactured Using the Space Holder Method for Bone Substitute Materials. *Metals* **2019**, *9*, 340. [CrossRef]

Publisher's Note: MDPI stays neutral with regard to jurisdictional claims in published maps and institutional affiliations.